

# Numerical study of double emulsion droplet generation in a dual-coaxial microfluidic device using response surface methodology

Amirmohammad Sattari<sup>a,b</sup>, Nishat Tasnim<sup>b</sup>, Pedram Hanafizadeh<sup>a,\*\*</sup>, Mina Hoorfar<sup>b,\*</sup>

<sup>a</sup> School of Mechanical Engineering, College of Engineering, University of Tehran, Iran

<sup>b</sup> School of Engineering, University of British Columbia, Kelowna, BC, V1V 1V7, Canada

## ARTICLE INFO

### Keywords:

Droplet microfluidics  
Double emulsion  
Physical properties  
Dual-coaxial  
Dripping instability

## ABSTRACT

This paper presents a parametric study using a three-phase axisymmetric numerical simulation on a dual co-axial microfluidic device for creating compound droplets. The Volume of Fluid-Continuum Surface Force model (VOF-CSF) was developed to perform a parametric analysis of the double emulsion formation in a dual co-axial microfluidic device. The model was used to investigate the effects of phase velocities, viscosities, and interfacial tensions on the size and generation rate of the double emulsions, with the assistance of the Design of Experiments (DOE) and Response Surface Methodology (RSM). The DOE considerably decreased the number of simulations. A sensitive analysis revealed that the outer phase parameters have the most noteworthy influence on double emulsion characteristics. Dimensionless numbers, including Weber number of the inner phase ( $We_{in}$ ), the capillary number of the middle phase ( $Ca_{mid}$ ), and the capillary number of the outer phase ( $Ca_{out}$ ), were also implemented to examine the effects of essential forces on the double emulsion size. The simulation results verified that the size of both the inner and the outer droplets could be easily adapted within a broad range by adjusting non-dimensional parameters. The simulation results can be utilized to generate a broad range of liquid-liquid encapsulated structures.

## 1. Introduction

Double emulsions are three-phase dispersions in which a liquid shell encapsulates one liquid droplet, which is further dispersed in another continuous phase. Due to the presence of the middle phase as a protective shell or semipermeable barrier separating the inner phase droplet from the continuous phase medium, double emulsions are suitable structures for a broad range of applications, including controlled delivery [1–3], food science [4,5], biotechnology [6,7], and cosmetics [8,9].

The procedure of double emulsion generation is generally based on the combinations of the most common microfluidic droplet generation strategies. These strategies can be categorized into three groups: (1) cross-junctions [10–12], (2) flow-focusing [13–16], and (3) co-flowing [17,18]. Glass capillary devices have been able to combine two consecutive co-flowing and flow-focusing strategies, and hence are one of the most common and effective methods for the production of monodispersed double emulsions with high throughput [19]. Utada et al. [14,20], were one of the leading groups to develop and characterize a

microcapillary device to study double emulsion formation. Their device could perform fluid encapsulation (with a high degree of control) and the quantitative prediction of droplet size from the flow profiles of the fluids. Other groups have improved the geometry of microcapillary devices for precise control of emulsion structures. For instance, Akamatsu et al. [21] developed a membrane-integrated glass capillary for producing water-in-oil-in-water (W/O/W) compound droplets, which was able to produce emulsions with ultra-thin shells. A similar geometry was employed by Nam et al. [22], in which they also injected Pt nanoparticles through the inner phase into the emulsion to make the structure active for catalyst applications.

Numerous experimental studies have been performed on drop formation in glass capillary devices with a focus on the impacts of fluid flow rates and geometry on the size and morphology of double emulsions [23–27], however, compared to the experimental works, there have been a very few numerical parametric studies devoted to double emulsion formation and transition from dripping to jetting regimes in microfluidics [28–33]. For instance, Zhou et al. [28] numerically investigated the formation of compound droplets in a 2D axisymmetric

\* Corresponding author.

\*\* Corresponding author.

E-mail address: [mina.hoorfar@ubc.ca](mailto:mina.hoorfar@ubc.ca) (M. Hoorfar).

flow-focusing geometry. They utilized finite elements with adaptive meshing and detected both dripping and jetting regimes in relatively low and high flow rates, respectively. The assumption of 2D axisymmetric geometry was doubtful for rectangular cross-sections flow-focusing device, and hence the results were not reliable. Another 2D axisymmetric simulation on double emulsion formation has been performed by Nabavi et al. [29] using the Volume of Fluid (VOF) method in combination with the Continuum Surface Force (CSF). Their structure was based on the combination of co-flowing and a flow-focusing. Although they performed a comprehensive study on the effects of various parameters, including phase flow rates, physical properties, and geometrical parameters, the effects of each parameter were investigated individually, which means they changed each parameter when the others were kept constant. So, they did not provide an in-depth understanding of the sensitivity of each parameter on the double emulsion characteristics. A few studies have presented three-dimensional (3D) simulations to investigate the effects of various parameters, including phase flow rates, fluid properties, and geometry of the capillaries on the characteristics of the double emulsion. For instance, a 3D simulation was developed by Azarmanesh et al. [31] for two consecutive flow-focusing devices used to generate and manipulate double emulsion droplets. They used Direct Numerical Simulation (DNS) using the finite volume method and adaptive mesh refinement technique. They studied influence of various non-dimensional groups on the characteristics of compound droplets and found a decussate regime of the double-emulsion/empty-droplet at low Weber numbers of the inner fluid. However, they only investigated effects of phase flow rates, and influences of other physical properties were missed in this study. Vu et al. [32] utilized the front-tracking method to study the influence of surface tension, phase velocities, and radius ratio on the characteristics of compound droplets in an axisymmetric co-flowing design, and found that the transition from dripping to jetting is profoundly affected by the flow rate ratios.

Unlike the limited number of modeling studies published for double emulsions, diverse approaches have been developed for the simulation of multiphase flow in microfluidics, which are generally classified into surface tracking methods and interface capturing methods [34]. The surface tracking method requires lattices for tracking the interfaces, which are updated at each time step [35,36]. In contrast, the interface-capturing method utilizes a continues function, which is usu-

ally called an "indicator function", to determine the different phases as well as the position of the interface [34]. This method demonstrates higher flexibility of handling topological changes and is, therefore, more suitable for droplet simulation [34]. Common interface capturing methods are the Level set method [37], phase-field method [38], and Volume of Fluid (VOF) method [39]. The VOF model, coupled with Continuum Surface Force (CSF) approach [40], has been reported to be a very promising method for the simulation of droplet microfluidics problems [29,41]. Furthermore, it is well-known that the VOF method is entirely independent of the density and viscosity ratios of phases or the phase flow Reynolds number [42], which makes this method applicable in a wide range of operating conditions. Besides, the surface properties can be readily adjusted in the VOF-CSF method in the wall boundary conditions [29,41].

$0 < \alpha_p < 1$  : The computational cell contains an interface between phase  $pth$  and one or more other phases

ally called an "indicator function", to determine the different phases as well as the position of the interface [34]. This method demonstrates higher flexibility of handling topological changes and is, therefore, more suitable for droplet simulation [34]. Common interface capturing methods are the Level set method [37], phase-field method [38], and Volume of Fluid (VOF) method [39]. The VOF model, coupled with Continuum Surface Force (CSF) approach [40], has been reported to be a very promising method for the simulation of droplet microfluidics problems [29,41]. Furthermore, it is well-known that the VOF method is entirely independent of the density and viscosity ratios of phases or the phase flow Reynolds number [42], which makes this method applicable in a wide range of operating conditions. Besides, the surface properties can be readily adjusted in the VOF-CSF method in the wall boundary conditions [29,41].

In this study, we performed a 2D axisymmetric simulation on a dual co-axial microfluidic device for the controllable generation of compound emulsions using the VOF-CSF approach. In total, eight parameters, including five physical parameters and three fluid flow rates, have been systematically varied utilizing the Design of Experiment (DOE)

## 2. Methodology

### 2.1. Governing equations

The governing equations consist of the conservation of mass, Eq. (1), and momentum, Eq. (2).

$$\frac{\partial \rho}{\partial t} + \nabla \cdot (\rho \vec{U}) = 0 \quad (1)$$

$$\frac{\partial}{\partial t} (\rho \vec{U}) + \nabla \cdot (\rho \vec{U} \vec{U}) = -\nabla P + \nabla \cdot [\mu (\nabla \vec{U} + \nabla \vec{U}^T)] + F_{st} \quad (2)$$

in which  $\rho$ ,  $t$ ,  $\vec{U}$ ,  $P$ , and  $\mu$  donate density, time, velocity vector, pressure, and dynamic viscosity, respectively.  $F_{st}$  is the surface tension force acting at the interface of two immiscible phases. The gravitational acceleration has been neglected since the length-scale is in the order of a few microns.

In the VOF model, an additional continuity equation is solved to track the interface for the volume fraction of Phase  $p$ .  $\alpha_p$  is a representation of the phase advection.

$$\frac{\partial \alpha_p}{\partial t} + \vec{U} \cdot \nabla \alpha_p = 0 \quad (3)$$

The portion of each computational cell filled with a specific phase is determined by the volume fraction of that phase using the following

conditions:

In the present model, subscribes 1, 2, and 3 refer to the inner, middle, and outer phases, respectively. The density and the dynamic viscosity are defined to vary smoothly over the interface by letting:

$$\rho = \alpha_1 \rho_1 + \alpha_2 \rho_2 + (1 - \alpha_1 - \alpha_2) \rho_3 \quad (5)$$

$$\mu = \alpha_1 \mu_1 + \alpha_2 \mu_2 + (1 - \alpha_1 - \alpha_2) \mu_3 \quad (6)$$

Employing the CSF method, the interfacial surface force,  $F_{st}$ , is calculated using the diffuse interface representation:

$$F_{st} = \sigma \kappa \nabla \alpha \quad (7)$$

where  $\sigma$  is the interfacial tension, and  $\kappa$  is the local curvature of the interface, which is calculated as follows:

$$\kappa = \nabla \cdot \hat{n} \quad (8)$$

where  $\hat{n}$  is the unit normal defined as,

$$\hat{n} = \frac{\nabla \alpha}{|\nabla \alpha|} \quad (9)$$

Despite the significant ability of the VOF model to capture the sharp interface, it has a few limitations including: (i) lack of compatibility with the density-based solvers (only the pressure-based solvers must be employed); (ii) the need for all control volumes to be filled with either a single fluid phase or a mixture of phases (the VOF model is not appropriate for void regions where no fluid of any type is available); (iii) the lack of ability of the VOF explicit scheme in applying the second-order implicit time-stepping formulation.

The VOF method can also be employed in conjunction with Fluid Solid Interaction (FSI) analysis. The coupling between an FSI and a VOF solver has significantly increased the ability to analyze a wide range of problems involving major applications such as filling [43], sloshing [44], and the study of tanks under earthquake loads [45]. In order to couple the two problems, various strategies have been proposed [46,47]; for instance, the first code output field can be printed on a file, and the other code can be performed with this file as an input and vice versa.

## 2.2. Non-dimensional numbers

The Weber number of the inner phase,  $We_{in}$ , and capillary numbers of the middle,  $Ca_{mid}$ , and outer phases,  $Ca_{out}$ , are considered as the non-dimensional groups.

$$We_{in} = \frac{\rho_{in} \cdot U_{in}^2 \cdot D_{in}}{\sigma_{12}} \quad (10)$$

$$Ca_{mid} = \frac{\mu_{mid} \cdot U_{mid}}{\sigma_{23}} \quad (11)$$

$$Ca_{out} = \frac{\mu_{out} \cdot U_{out}}{\sigma_{23}} \quad (12)$$

In the above relations,  $\rho$ ,  $\sigma$ ,  $\mu$ ,  $U$ , and  $D$  denote density, interfacial tension, viscosity, superficial velocity, and droplet diameter, respectively. Subscripts *in*, *mid*, and *out* refer to the inner, middle, and outer phases, respectively. Also,  $\sigma_{12}$  and  $\sigma_{23}$  are interfacial tensions between the internal and middle and the middle and external phases, respectively.

## 2.3. Numerical method

The geometry of the microfluidic device consists of three nested capillary tubes, shown in Fig. 1 along with the boundary conditions and the meshed domain. The inner, middle and outer capillary tubes have the same axis and different internal diameters of 20, 60, and 120  $\mu\text{m}$ , respectively. The tips of the inner and middle capillaries are precisely placed in the same position. The length of the main capillary tube is 20 times longer than the outer capillary diameter to eliminate the influence of the outlet boundary.

A 2D axisymmetric, time-dependent pressure-based segregated algorithm in the finite volume based Ansys® Fluent 19.2 commercial software was developed to perform the parametric analysis on compound droplet formation. The discretized momentum equation was approximated employing the QUICK scheme to get the most accurate solution. The pressure term interpolation was obtained by the PRESTO scheme in which the pressure term was directly calculated on the interfaces, and interpolation errors were avoided [29]. The pressure-velocity coupling was accomplished by the SIMPLE scheme, and the interface interpolation was performed by the Geo-Reconstruction algorithm. A variable time step method using the maximum Courant number,  $Co_{max}$ , with the prescribed value of 0.35, was employed to reduce the computational cost.

All three inlets were specified using constant inlet velocities. The outlet boundary was determined as the pressure outlet. All other boundaries were imposed with the non-wetted wall conditions because the encapsulated structure in the designed geometry was not influenced by the wettability of the outer wall.

Three different cases based on mesh resolutions of 10, 5, and 2  $\mu\text{m}$  were considered in order to investigate the grid dependency effect. Since no significant differences in the behavior and characteristics of compound droplets were observed for the resolutions of 5 and 2  $\mu\text{m}$ , considering computational cost and a large number of simulations, a fine mesh with a resolution of 5  $\mu\text{m}$  was implemented for all simulations.

## 2.4. Model validation

Although several studies have verified the accuracy of the VOF model, here, we present a qualitative comparison of our model with experiments conducted by Shao et al. [48] (Fig. 2). Their double emulsion generation consisted of two main parts, including a supporting body and three co-axial capillaries. In this configuration, the inner fluid

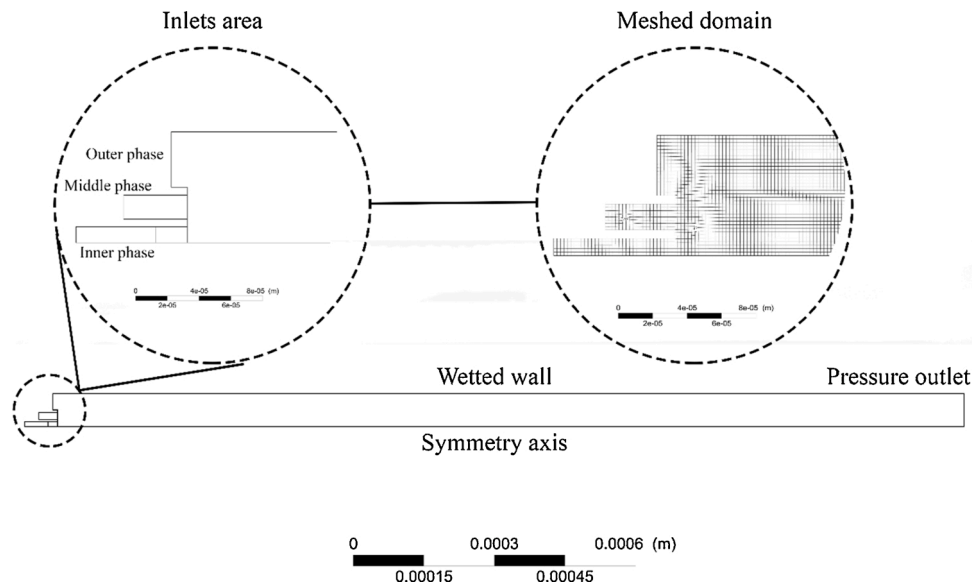
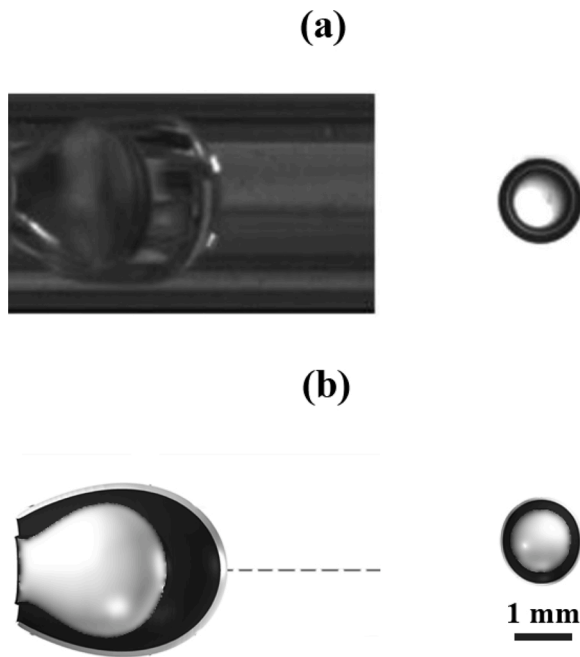


Fig. 1. Schematic view of the two co-axial geometry for the preparation of double emulsions along with boundary conditions and the meshed domain.



**Fig. 2.** (a) Experimental study of Shao et al. [48] (Reproduced from [40] with permission from Elsevier, Copyright © 2013 Elsevier Ltd), and (b) numerical simulation of the compound droplet formation (The corresponding conditions are  $Q_i + Q_m = 200 \mu\text{l/min}$ ,  $Q_i/Q_m = 2$ , and  $Q_o = 2000 \mu\text{l/min}$ ). (Left) Near breakup moment; (Right) after the breakup.

is injected through the innermost capillary tube into the middle capillary, which together are injected into the outer capillary. The double emulsion is then created at the downstream of the outer capillary as a result of dripping instability. They also utilized a high-speed camera with a recording frequency of 200 fps mounted to a zoom lens to record the generation of double emulsions. Our numerical model could accurately predict the compound droplet formation process both before (Fig. 2a) and after (Fig. 2b) breakup. The inner and outer droplet diameters of the numerical simulation were  $1403 \mu\text{m}$  and  $1983 \mu\text{m}$ , respectively, while the experimental measurements revealed diameters of  $1433 \mu\text{m}$  and  $2003 \mu\text{m}$ , respectively. Hence, the errors are approximately 2% and 1% for the inner and outer droplet diameters, respectively. The corresponding operation conditions are  $Q_i + Q_m = 200 \mu\text{l/min}$ ,  $Q_i/Q_m = 2$ , and  $Q_o = 2000 \mu\text{l/min}$ , where  $Q_i$ ,  $Q_m$ , and  $Q_o$  are the inner, middle, and outer phases flow rates, respectively.

**Table 1**  
The range of input parameters for the design of experiment study.

Parameter	Symbol	Unit	Range
Inner phase velocity	$U_{in}$	m/s	0.01 – 0.1
Middle phase velocity	$U_{mid}$	m/s	0.01 – 0.1
Outer phase velocity	$U_{out}$	m/s	0.05 – 0.5
Inner phase viscosity	$\mu_{in}$	Pa.s	0.025–0.1
Middle phase viscosity	$\mu_{mid}$	Pa.s	0.025–0.1
Outer phase viscosity	$\mu_{out}$	Pa.s	0.007–0.08
The interfacial tension between inner and middle phases	$\sigma_{12}$	N/m	0.005–0.06
The interfacial tension between middle and outer phases	$\sigma_{23}$	N/m	0.025–0.1
Inner phase density	$\rho_{in}$	kg/m <sup>3</sup>	1180
Middle phase density	$\rho_{mid}$	kg/m <sup>3</sup>	1170
Outer phase density	$\rho_{out}$	kg/m <sup>3</sup>	1200

## 2.5. Design of experiment (DOE)

The DOE method provides an efficient and statistical approach to obtain desirable results. Contrary to traditional experimentation (which varies one-factor-at-a-time (OFAT)), the DOE method changes multiple variables simultaneously, allowing the assessment of interactions between variables [49]. Response Surface Method (RSM) is one of the well-known formal experimental plans in which quantitative independent variables will be related to the response variables utilizing some statistical models [49].

Here we considered three phase inlet velocities and five physical properties, including viscosities and interfacial tensions between phases, as the input parameters to our DOE. The range of input parameters is tabulated in Table 1. Note that the densities of phases were ignored as the input parameters since it was found that they do not have a significant effect on the formation process and characteristics of double emulsions [29]. This assumption led to a significant reduction in the number of design points from 242 to 82 using the Central Composite Design (CCD) scheme. CCD has been utilized widely along with RSM to design and optimize different problems in various fields of studies and has been demonstrated to be a robust and efficient approach [50,51]. Here, we implemented a full second-order polynomials model [52] as the response surface type, which is widely used in RSM due to its high accuracy in solving real response surface problems [53].

The inner and outer droplet diameters and double emulsion frequency of formation have been considered as the output parameters. The goodness of the fit plot for droplet diameters, illustrated in Fig. 3 compares the results obtained by the response surface method to those observed from design points. The results show a coefficient of determination of 0.94 and 0.93 for inner and outer droplet diameters, respectively, which are appropriate values for a response surface study [54].

## 3. Results and discussion

### 3.1. Dripping regime

The formation of the double emulsions in the asymmetrical geometry is simulated within two same-level co-axial arrangements. For dripping regime, the inner fluid is injected through the internal channel into the forming droplet of the middle phase, which results in the creation of the

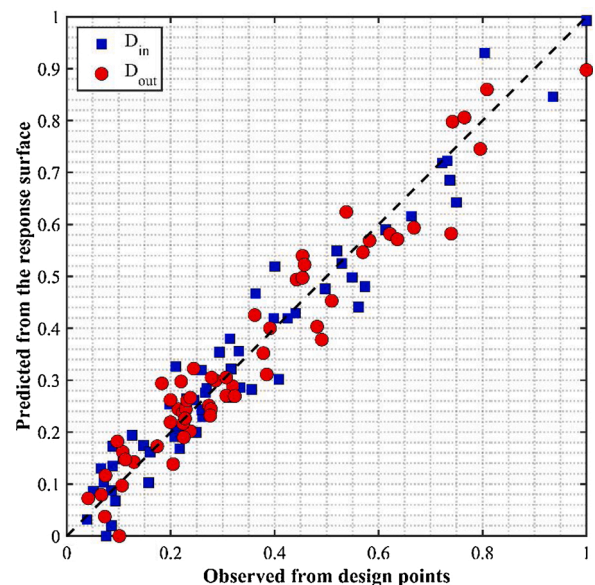


**Fig. 3.** A comparison between data gathered from the response surface study and data observed from the design points.



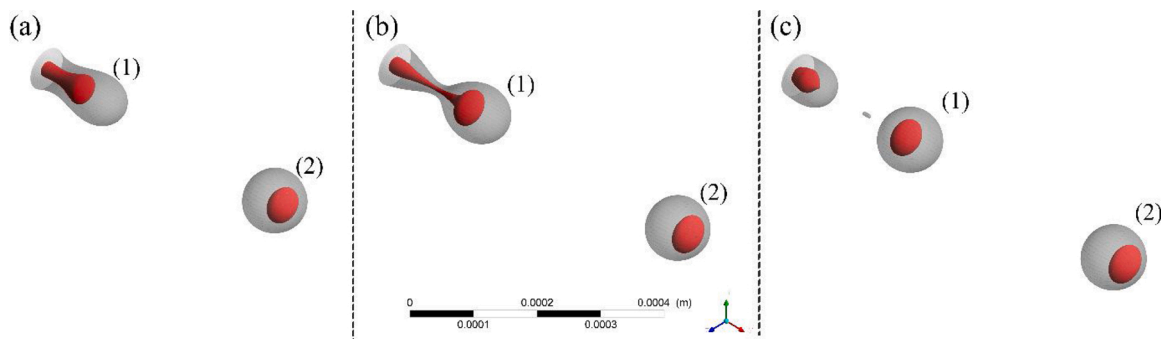


**Fig. 4.** Steps of double emulsion formation in dripping regime. (a) The filament of the inner phase is moving inside, forming a droplet of the middle phase ( $t = 8.34$  ms). (b) The inner phase filament then penetrates the middle phase droplet while it is in the necking process ( $t = 9.08$  ms). (c) The outer droplet breaks up due to the dripping instability, and the double emulsion is created ( $t = 9.49$  ms). ((1) and (2) refer to the first and second compound droplets, respectively). The corresponding operation conditions are  $U_{in} = 0.05$  m/s,  $U_{mid} = 0.05$  m/s,  $U_{out} = 0.1$  m/s,  $\mu_{in} = 0.0396$  Pa.s,  $\mu_{mid} = 0.0648$  Pa.s,  $\mu_{out} = 0.0482$  Pa.s,  $\sigma_{12} = 0.00574$  N/m, and  $\sigma_{23} = 0.095$  N/m.

inner phase liquid filament (Fig. 4a). The inner filament then penetrates the forming droplet of the middle phase (Fig. 4b). Finally, as a result of dripping instability, the double emulsion droplet is generated at the downstream end of the main channel (Fig. 4c). When it reaches the downstream of the microchannel, the outer droplet diverges from the spherical shape due to the higher momentum of the inner droplet, which tends to accelerate it towards the outer tip of the droplet.

### 3.2. Jetting regime

When the flow rate of the dispersed phase increases, the formation of the droplet changes to the jetting regime, and the fluid filament is breaking up downstream of the channel through a jet instability process. It is well-known that when the capillary number of the continuous phase is small, the dripping regime occurs because of the domination of the surface tension over viscous forces. When the continuous phase capillary becomes larger, the viscous shear force is the dominant force, and the jetting regime happens. The procedure of double emulsion formation is almost similar to that of the dripping regime, i.e., the inner jet stream penetrates the forming jet of the middle phase (Fig. 5a), the necking process results in breaking up the internal jet stream into single or multiple droplets (Fig. 5b), and the outer jet stream also breaks up into several droplets, which encapsulate inner droplets (Fig. 5c).

### 3.3. Widening jet regime

The droplet formation in both dripping and jetting regimes can be explained by employing various instability theories. The

Rayleigh–Plateau [55] is one of the most well-known theories, explaining why/how a liquid filament breaks up into smaller droplets with an equivalent volume but a smaller surface area. The absolute instability occurs when the instability in the fluid thread advances in both downstream and upstream [56]. This situation is designated as the dripping regime because instabilities invade the entire jet, particularly the injecting orifice outlet. Conversely, suppose all developing instabilities travel downstream. In this case (i.e., called convective [56]), the jetting regime happens, in which the fluid velocity is relatively high to advect the instabilities causing the breakup phenomenon away from the orifice tip.

In addition to the two common flow regimes in co-flowing devices (dripping and jetting regimes), another flow regime very similar to the jetting with some minor differences has been identified. This flow regime is called widening jet regime [30]. In such a regime, the tip of the formed jet has a widening shape, resulting from the higher velocity of the middle phase compared to that of the outer phase [29]. Therefore, the larger shear rate at the interface due to the larger velocity difference decelerates the liquid jet, provoking it to widen [57]. In this flow regime, the double formation procedure is similar to the previous regimes (Fig. 6). The only difference compared to the jetting regime is that the filament breakup is followed by a single droplet formation (there is a larger droplet at the tip of the liquid filament). It should be noted that the monodispersity of this flow regime is generally smaller than the dripping regime due to the higher and more irregular instabilities acted on both interfaces.

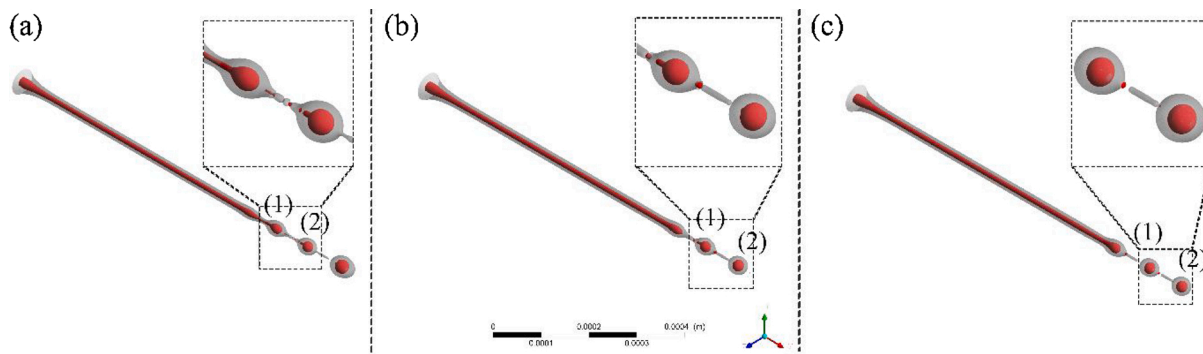


**Fig. 5.** Steps of double emulsion formation in the jetting regime. (a) The jet of the inner phase is moving inside of the forming jet of the middle phase ( $t = 9.24$  ms). (b) The jet of the inner phase breaks up into several droplets inside the forming jet of the middle phase ( $t = 9.31$  ms). (c) The outer jet breaks up due to jetting instability, resulting in the formation of double emulsions ( $t = 9.41$  ms). ((1) and (2) refer to the first and second compound droplets, respectively). The corresponding operation conditions are  $U_{in} = 0.055$  m/s,  $U_{mid} = 0.055$  m/s,  $U_{out} = 0.275$  m/s,  $\mu_{in} = 0.0505$  Pa.s,  $\mu_{mid} = 0.046$  Pa.s,  $\mu_{out} = 0.0435$  Pa.s,  $\sigma_{12} = 0.00574$  N/m, and  $\sigma_{23} = 0.05$  N/m.

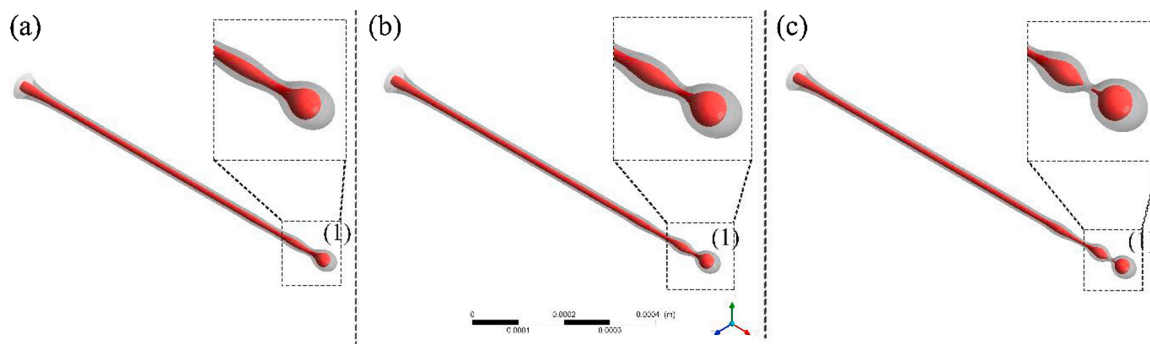


**Fig. 6.** Steps of double emulsion formation in widening the jet regime. (a) The jet of the inner phase is moving inside the widening jet of the middle phase ( $t = 9.43$  ms). (b) The jet of the inner phase penetrates the middle phase widening jet while the necking process happens ( $t = 9.64$  ms). (c) The outer widening jet breaks up due to the fluid instability, and the double emulsion is created ( $t = 9.84$  ms). ((1) refers to formation of compound droplets). The corresponding operation conditions are  $U_{in} = 0.077$  m/s,  $U_{mid} = 0.033$  m/s,  $U_{out} = 0.39$  m/s,  $\mu_{in} = 0.0258$  Pa.s,  $\mu_{mid} = 0.0679$  Pa.s,  $\mu_{out} = 0.0253$  Pa.s,  $\sigma_{12} = 0.0193$  N/m, and  $\sigma_{23} = 0.0276$  N/m.

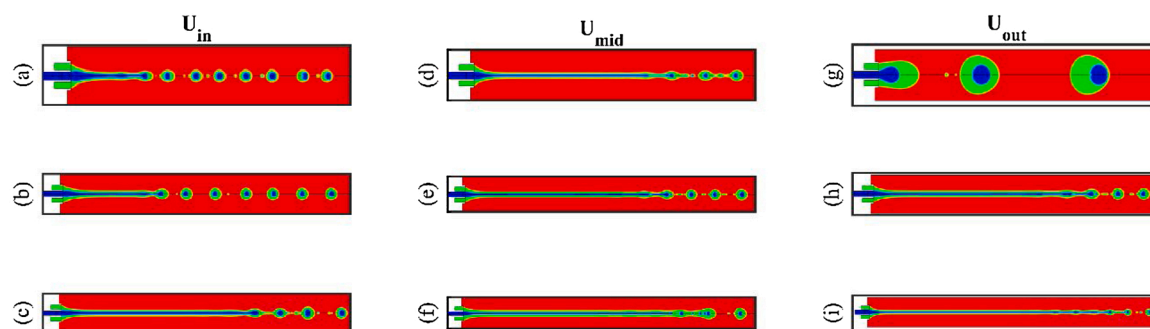


**Fig. 7.** Effects of (a-c) inner phase velocity ((a)  $U_{in} = 0.01$  m/s, (b)  $U_{in} = 0.055$  m/s, (c)  $U_{in} = 0.1$  m/s), (d-f) middle phase velocity ((d)  $U_{mid} = 0.01$  m/s, (e)  $U_{mid} = 0.055$  m/s, (f)  $U_{mid} = 0.1$  m/s), and (g-i) outer phase velocity ((g)  $U_{out} = 0.05$  m/s, (h)  $U_{out} = 0.1$  m/s, (i)  $U_{out} = 0.5$  m/s) on the double emulsion formation. The corresponding conditions are  $\mu_{in} = 0.0629$  Pa.s,  $\mu_{mid} = 0.0570$  Pa.s,  $\mu_{out} = 0.0435$  Pa.s,  $\sigma_{12} = 0.0326$  N/m, and  $\sigma_{23} = 0.0661$  N/m.

### 3.4. Effect of phase flow rates

The contours of volume fraction in various phase velocities are demonstrated in Fig. 7. Generally, increasing each phase flow rate leads to greater elongation of both inner and middle phase jets. Increasing the inner phase velocity increase both the inner and outer droplet sizes (Fig. 7a-c). In contrast, an increase in middle phase velocity leads to an increase in the outer droplet size and a reduction in the inner droplet diameter (Fig. 7d-f). Increments in the outer phase velocity decreased the size of the inner and outer droplets dramatically (Fig. 7g-i), causing the transition of the double formation regime from dripping to jetting (Fig. 7g and h).

The quantitative effects of phase flow rates on the inner phase equivalent diameter ( $D_{in}$ ) and frequency of formation ( $f$ ) are illustrated as the response surfaces in Fig. 8a-d. An increase in innermost velocity leads to a rise in the inner phase droplet diameter at any middle or outer phase velocities (Fig. 8a and b). This is due to the increase in both inertial and viscous forces of the inner phase fluid, which means more surface tension force is required to predominate inertia and viscous forces for the breakup process that is obtained by larger droplets in constant surface tension conditions. A more significant inner phase velocity also moves the breakup location to the downstream of the main channel, which results in a more stretched internal phase jet (Fig. 7a-c). Increasing the middle phase velocity does not have a noticeable effect on the inner droplet diameter at any of the inner phase velocities (Fig. 8a) and only reduces  $D_{in}$  slightly. The increase in the middle phase velocity results in higher velocity gradients at the internal interface, and thus increases the shear stress exerted by the intermediate phase to the inner interface, leading to the smaller inner droplets. This influence is more significant at lower outer phase velocities (Fig. 8c), in which the breakup

process of the inner droplet is mostly influenced by the shear stress applied by the middle phase.

Increasing the outer phase velocity has the most notable control over the inner droplet size, and reduces it regardless of any inner and middle phase velocities (Fig. 8b and c). The influence is more noticeable in the smaller middle phase velocities (Fig. 8c). The reduction in the inner droplet diameter is mainly due to the increase in shear stress applied by the outer phase stream to the middle phase jet interface. Increasing the outer phase velocity leads to the suppression of the middle phase jet (Fig. 7h and i), which also reduces the formation time and results in the formation of a smaller droplet. Due to the opposite effects of the inner and middle phase velocities on the inner droplet size, the response surface of formation frequency as functions of  $U_{in}$  and  $U_{mid}$  has a dome-shaped behavior, which means it will have a maximum point somewhere in the mid-range of the mentioned parameters (Fig. 8d).

The response surfaces of the outer droplet equivalent diameter ( $D_{out}$ ) and frequency of formation ( $f$ ) against the phase flow rates are demonstrated in Fig. 8e-h. The inner phase velocity has different impacts on  $D_{out}$  in relatively small and large values of the middle phase velocity, i.e.,  $D_{out}$  is reduced with an increase in the internal phase velocity in the range of  $U_{mid} < \sim 0.055$  (m/s), while they have a direct relationship for  $U_{mid} > \sim 0.055$  (m/s) (Fig. 8e). At relatively small middle phase velocities ( $U_{mid} < \sim 0.055$  (m/s)), the higher inner phase velocity values produce steeper velocity gradients and higher shear stress exerted by the internal phase to the external interface, which facilitates the detachment process and results in smaller droplet size. However, at larger middle phase velocities ( $U_{mid} > \sim 0.055$  (m/s)), the increment in the velocity gradient by the inner phase does not have a notable influence on the shear stress exerted on the external interface. Hence, the outer phase droplet size increment may be attributed to a delay arising

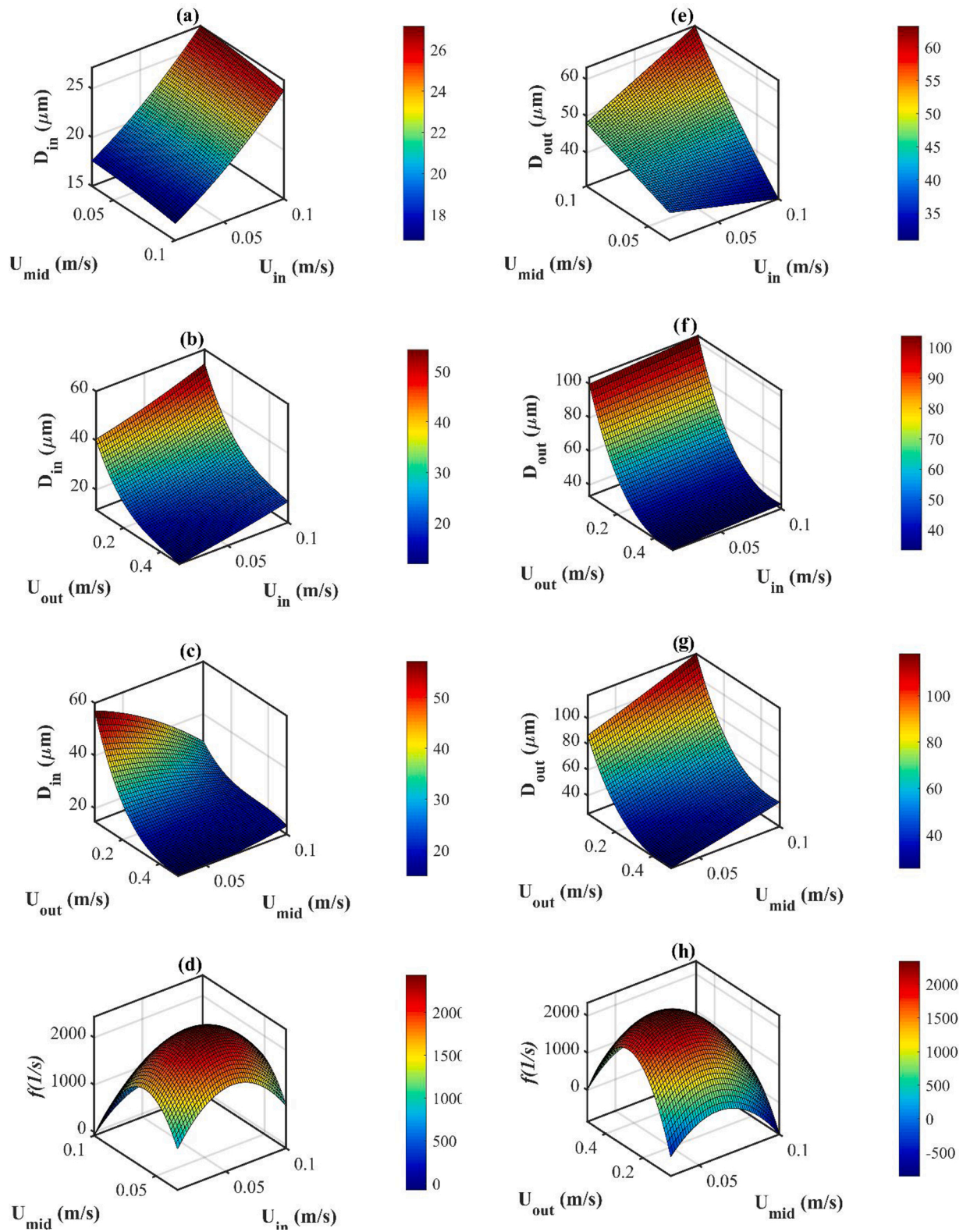


**Fig. 8.** (a-d) Effect of the (a) inner and middle phase velocity, (b) inner and outer phase velocity, and (c) middle and outer phase velocity on the inner phase droplet equivalent diameter. (d) Influence of the middle and outer phase velocities on the frequency of compound droplet formation. (e-h) Effect of the (e) inner and middle phase velocity, (f) inner and outer phase velocity, and (g) middle and outer phase velocity on the outer phase droplet equivalent diameter. (h) Influence of middle and outer phase velocities on the frequency of compound droplet formation. The corresponding operating conditions are  $\mu_{in} = 0.0629 \text{ Pa.s}$ ,  $\mu_{mid} = 0.0570 \text{ Pa.s}$ ,  $\mu_{out} = 0.0435 \text{ Pa.s}$ ,  $\sigma_{12} = 0.0326 \text{ N/m}$ , and  $\sigma_{23} = 0.0661 \text{ N/m}$ .

from the blockage of the middle phase jet necking process by the inner jet stream, which delays the detachment and results in larger droplets.

Increasing the middle phase velocity results in larger outer droplets regardless of  $U_{in}$  and  $U_{out}$  operating ranges (Fig. 8e and f). There is a similar justification regarding the effect of the inner phase velocity on the inner droplet diameter: increasing  $U_{out}$  reduces  $D_{out}$  dramatically in any ranges of  $U_{in}$  and  $U_{mid}$  (Fig. 8f and g) as a result of the shear stress growth at the outer interface due to an increase in the velocity gradient, which facilitates breakup of the middle phase jet. It also has a more significant influence on the droplet size than the inner and middle phase velocities; as a result, the shear stress at the outer interface impacts the middle phase jet more significantly than the inner interface. A dramatic reduction in the droplet size at the lower outer velocity is related to the transition from the dripping to the jetting regime (Fig. 7g and h). As discussed earlier, due to the opposite effects of the middle and outer phase velocities on the outer droplet size, the response surface of the formation frequency has a dome-shaped behavior (Fig. 8d).

### 3.5. Effect of phase physical properties

The contours of the volume fraction for diverse phase physical properties are shown in Fig. 9. It can be observed that generally, increasing the phase viscosities results in greater elongation of both inner and middle phase jets (Fig. 9a-i); while increasing both  $\sigma_{12}$  and  $\sigma_{23}$  suppresses the inner and outer fluids jetting (Fig. 9j-o).

As illustrated in Fig. 10a-c, the outer droplet diameter is almost unaffected by  $\mu_{in}$  due to the poor influence of  $\mu_{in}$  on the shear stress acted on the outer interface. However, the influence of  $\mu_{in}$  on the inner droplet diameter is significant, i.e., an increase in  $D_{in}$  can be seen as  $\mu_{in}$  increases from 0.02 to 0.1 Pa.s. An increase in  $\mu_{in}$  ( $\mu_{in} > 0.05$  Pa.s) also causes the inner phase formation to transit from the dripping to jetting regimes due to the growth in the capillary number of the internal phase. As discussed earlier, an increase in the capillary number results in the domination of viscous forces and elongation of the liquid filament, which corresponds to the jetting regime.

Increasing  $\mu_{mid}$  as shown in Fig. 9d-f, leads to an increase in the both inner and outer filament lengths and transition from dripping to jetting. The increment in the ligament lengths is due to the increase in the

middle phase capillary and domination of the viscous over the interfacial tension forces. The increase in the shear stress due to the increase in the capillary number leads to the stretch of both liquid jets in the downstream of the channel.

The outer phase viscosity has the most significant influence on both inner and outer liquid filaments, according to Fig. 9g-i. An increase in  $\mu_{out}$  leads to an increase in the capillary number of the outer phase, as both velocity and interfacial tension remain constant. The higher capillary number leads to the higher shear force acting on the outer interface, resulting in elongation of both inner and middle phase filaments and transition from the dripping to jetting regimes ( $\mu_{out} > 0.007$  Pa.s). This higher level of viscous force accelerates the formation of droplets, leading to a higher frequency of formation and smaller inner and outer droplet diameters.

The effect of interfacial tension between the inner and middle phases,  $\sigma_{12}$ , is shown in Fig. 9j-l. Starting from  $\sigma_{12} = 0.00574$  N/m, both inner and middle phases are formed in the jetting regime. Increasing  $\sigma_{12}$  results in the reduction in the capillary number of the inner phase, which corresponds to the higher interfacial force compared to the viscous shear force. Hence, there is a tendency to retrograde the forming jet to the orifice tip. This causes the formation process to transit from the jetting regime to the dripping regime ( $\sigma_{12} > 0.06$  N/m). A similar procedure can be observed as a result of increasing the interfacial tension between the middle and outer phases ( $\sigma_{23}$ ), as it is shown in Fig. 9m-o. The interfacial tension force acting on the intermediate phase jet interface increases with increasing  $\sigma_{23}$ , which implies a reduction in the outer phase capillary number and domination of the interfacial tension over viscous shear forces. Higher values of the interfacial tension suppress the jets of both inner and middle phases and approach the formation process to the dripping regime.

Generally, the viscosity of the outer phase and the interfacial tension between the inner and middle phases have the most significant influence on the double emulsion formation process. It can also be concluded that choosing appropriate physical properties is essential in successive production of double emulsions, e.g., at a relatively small interfacial tension between the middle and outer phase fluids ( $\sigma_{23} = 0.005$  N/m), the outer jet stream along with the inner phase jet extends for a long distance to the outlet of the channel, and the double emulsion structure may not be

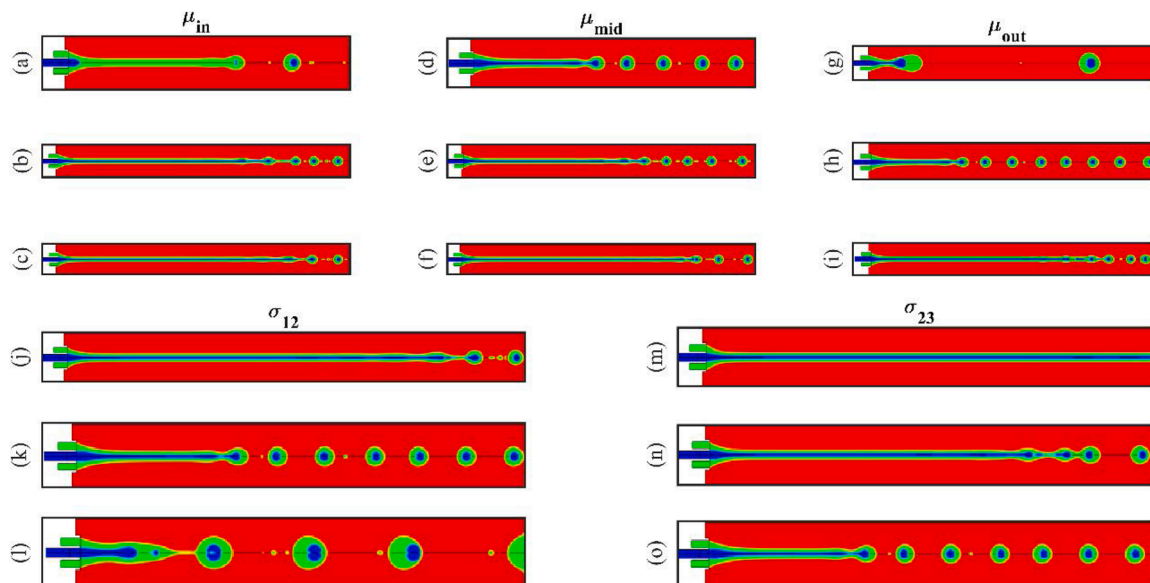


**Fig. 9.** Effect of the (a-c) inner phase viscosity ((a)  $\mu_{in} = 0.02$  Pa.s, (b)  $\mu_{in} = 0.05$  Pa.s, (c)  $\mu_{in} = 0.1$  Pa.s), (d-f) middle phase viscosity ((d)  $\mu_{mid} = 0.024$  Pa.s, (e)  $\mu_{mid} = 0.046$  Pa.s, (f)  $\mu_{mid} = 0.09$  Pa.s), (g-i) outer phase viscosity ((g)  $\mu_{out} = 0.007$  Pa.s, (h)  $\mu_{out} = 0.044$  Pa.s, (i)  $\mu_{out} = 0.08$  Pa.s), (j-l) interfacial tension between the inner and middle phases ((j)  $\sigma_{12} = 0.00574$  N/m, (k)  $\sigma_{12} = 0.03287$  N/m, (l)  $\sigma_{12} = 0.06$  N/m), and (m-p) interfacial tension between the middle and outer phases ((m)  $\sigma_{23} = 0.005$  N/m, (n)  $\sigma_{23} = 0.05$  N/m, (o)  $\sigma_{23} = 0.095$  N/m) on the double emulsion formation. The corresponding phase velocities are  $U_{in} = 0.05$  m/s,  $U_{mid} = 0.05$  m/s, and  $U_{out} = 0.1$  m/s.



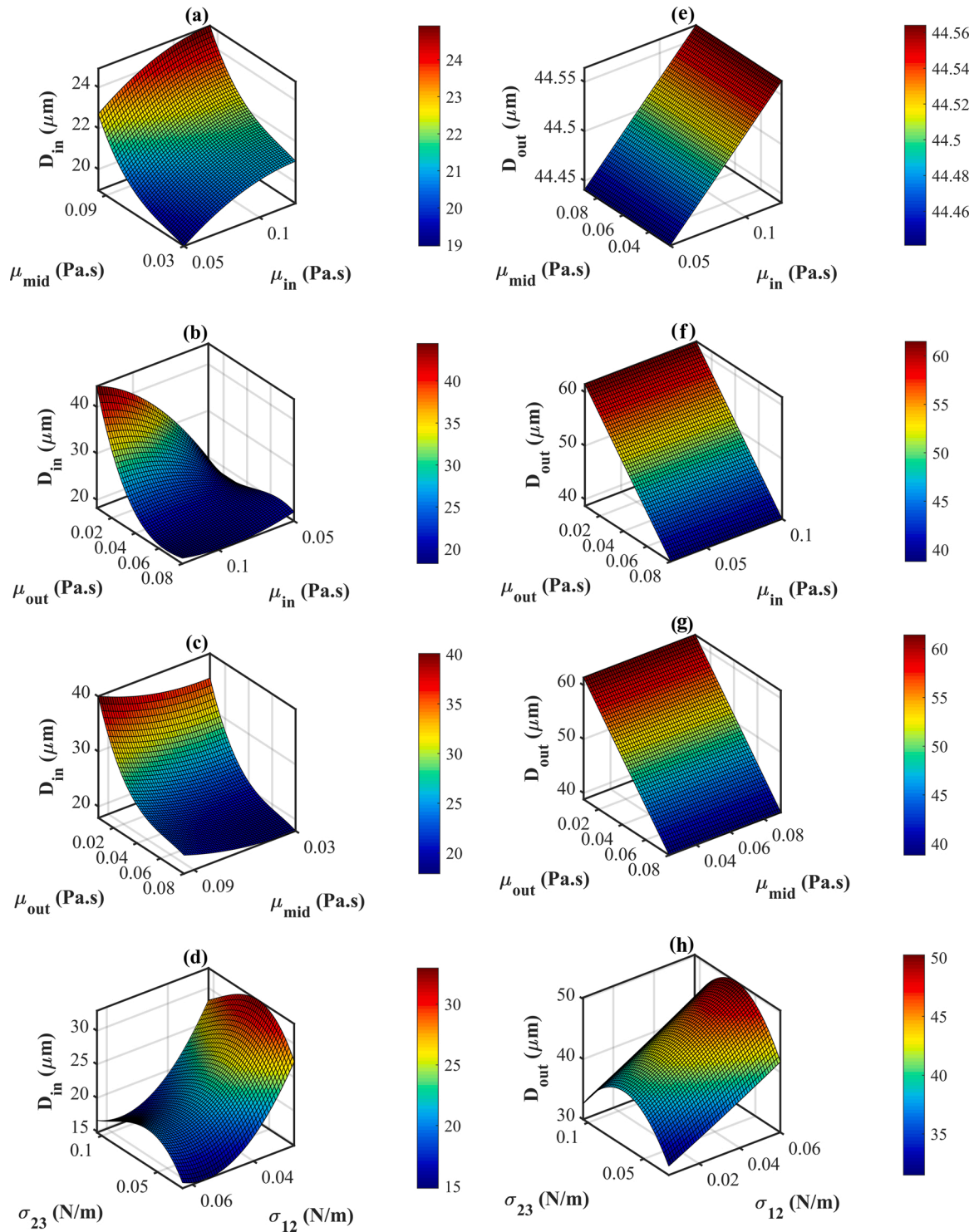


**Fig. 10.** (a-d) Effect of (a) inner and middle phase viscosity, (b) inner and outer phase viscosity, (c) middle and outer phase viscosity, and (d) influence of  $\sigma_{12}$  and  $\sigma_{23}$  on the inner phase equivalent diameter. (e-h) Effect of (e) inner and middle phase viscosity, (f) inner and outer phase viscosity, (g) middle and outer phase viscosity, and (h) influence of  $\sigma_{12}$  and  $\sigma_{23}$  on the outer phase equivalent diameter. The corresponding phase velocities are  $U_{in} = 0.05$  m/s,  $U_{mid} = 0.05$  m/s, and  $U_{out} = 0.1$  m/s.

formed (Fig. 9m).

The effects of the phase physical properties on the inner phase droplet diameter are demonstrated in Fig. 10a-d. Generally, variations of both  $\mu_{in}$  and  $\mu_{mid}$  do not have a noticeable influence on the inner droplet size (Fig. 10a, b, and c). Nevertheless, increasing both  $\mu_{in}$  and  $\mu_{mid}$  causes the internal jet to postpone the breakup location to the downstream of the channel and creates relatively large inner droplets. An increase in  $\mu_{in}$  follows with the domination of the viscous forces over surface tension,

which causes a longer inner jet filament and larger detached droplets, due to the requirement of a larger surface tension force to confer the viscous stress. The increase in  $\mu_{mid}$ , on the other hand, leads to an increase in the viscous stress on the inner fluid, causing the inner jet to stretch in the downstream of the channel. This results in the formation of larger droplets, as discussed earlier.

The outer phase viscosity has the most significant influence on the inner droplet size, i.e., increasing  $\mu_{out}$  leads to a dramatic reduction in

$D_{in}$ . Increasing  $\mu_{mid}$  leads to an increase in the viscous force acting on the external interface, which suppresses both liquid jets and causes both inner and outer jet ligaments to be stretched farther (Fig. 9g-i). The higher level of this viscous stress leads to more suppressed liquid jets, and hence a smaller droplet size (Fig. 10b and c).

Increasing  $\sigma_{12}$  causes a higher interfacial force in comparison with the shear force of the inner jet. Thus, there is an increasing tendency towards the dripping regime (Fig. 9l). Consequently, the inner jet breaks up faster, leading to smaller inner droplets (Fig. 10d). Two different behaviors can be observed regarding the influence of  $\sigma_{23}$  on the inner droplet diameter. At  $\sigma_{23} = 0.02 - 0.05 \text{ N/m}$ , an increase in  $\sigma_{23}$  delays the pinch-off mechanism and results in larger inner droplet sizes, while at higher  $\sigma_{23}$  ( $\sigma_{23} = 0.05 - 0.1 \text{ N/m}$ ), the inner droplet shrinks, causing the smaller inner droplet diameter. This may be due to the transition of the inner jet stream from the narrowing to widening jet regimes (Fig. 9m-o), which was also observed by [29].

The effects of the phase physical properties on the outer phase droplet diameter are shown in Fig. 10e-h. As can be seen,  $D_{out}$  is almost unaffected by the inner phase viscosity due to the negligible effect of  $\mu_{in}$  on the shear stress exerted to the external interface (Fig. 10a and b). Moreover, the middle phase viscosity has a negligible effect on the outer droplet diameter (Fig. 10b and c). This phenomenon was pointed out by [29,58], who declared that the droplet size and formation time are insensitive to the middle phase viscosity for a specific range of viscosity ratios ( $\mu_{out}/\mu_{mid}$ ). An increase in  $\mu_{out}$ , has the most considerable effect on outer droplet diameter, like the influence on the inner droplet, due to an increase in the shear stress applied by the external phase to the outer interface (Fig. 10b and c). Increasing  $\mu_{out}$  also leads to the transition from the dripping to jetting regime due to the higher viscous force being exerted on the external interface, which results in stretching both the inner and middle jets (Fig. 9g-i).

Increasing  $\sigma_{12}$  leads to an increase in the outer droplet diameter (Fig. 10d). It was explained that the more interfacial tension between the inner and middle phase tends to suppress both the inner and outer jetting and switch the droplet formation to the dripping regime (Fig. 9l). Similar to the influence of  $\sigma_{23}$  on the inner droplet diameter, two different behaviors on the outer droplet diameter were observed: at  $\sigma_{23} = 0.02 - 0.05 \text{ N/m}$ , an increase in  $\sigma_{23}$  delays the pinch-off event and results in larger outer droplet diameters, while at larger amounts,  $\sigma_{23} = 0.05 - 0.1 \text{ N/m}$ , the outer droplet shrinks, causing an increase in the droplet generation rate and resulting in smaller outer droplets.

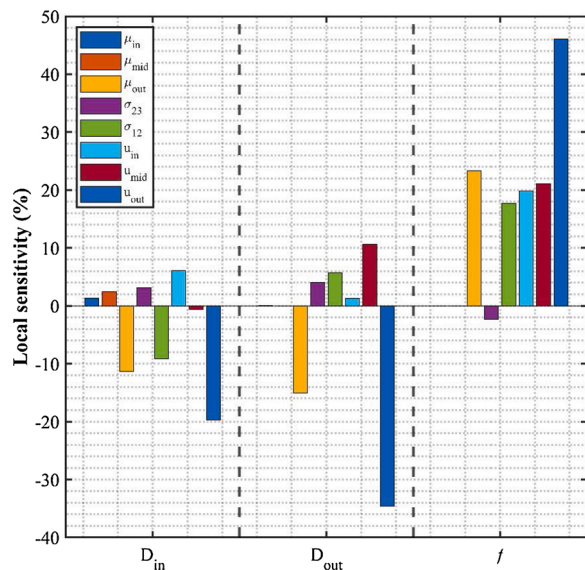


Fig. 11. Local sensitivity of input parameters on the characteristics of the compound droplets, including  $D_{in}$ ,  $D_{out}$ , and  $f$ .

### 3.6. Sensitivity analysis

The sensitivity of the compound droplet characteristics with regards to the input parameters is presented in Fig. 11. Local sensitivity analysis evaluates the local impact of input factors' variation on the model response by focusing on the sensitivity in the vicinity of a set of factor values. Such sensitivity is evaluated through partial derivatives of the output parameters at these factor values, i.e., the values of other input parameters are kept constant when examining an input factor's local sensitivity.

As can be seen, the outer phase parameters, including velocity and viscosity, generally have the most significant influence among other parameters. The input velocity has a small impact on the outer droplet diameter, a moderate influence on the inner droplet diameter, and a considerable effect on the frequency of formation. The results also demonstrate that the interfacial tensions have a moderate impact on all output parameters. Additionally, the results show that the inner phase parameters have no significant impact on the outer droplet diameter and frequency of formation, indicating that the internal droplet size can be tuned independently just by changing the inner phase parameters. However, varying the outer droplet diameter and frequency of formation by altering the input parameters led to a change in the inner droplet diameter as well.

Generally, the results of the sensitivity analysis revealed that a precise consideration of the phase parameters and velocities is essential for the production of desired size double emulsions in microfluidic systems. The accurate control on the size of the inner droplet can be achieved only by the tuning the velocity and viscosity of the internal phase; however, independent controlling of the outer droplet diameter is an arduous procedure since changing any parameter, including flow rates and physical properties of the inner and middle phases can also affect inner droplet characteristics.

### 3.7. Effect of non-dimensional groups

Non-dimensional groups, including Weber number of the inner phase, and capillary numbers of the middle and outer phases, are selected to perform the parametric study from the viewpoint of the effective forces acting on compound droplets (Fig. 12). It is observed that increasing  $We_{in}$  leads to the larger inner and outer droplets (Fig. 12a). An increase in  $We_{in}$  means the domination of fluid's inertia, which tends to elongate the fluid stream more, compared to its surface tension, which tends to break up the liquid filament. As a result, any increase in  $We_{in}$  results in the formation of larger inner droplets. The larger outer droplets may be due to the fact that the external droplet formation time increases since the more extended internal liquid jet due to higher values of  $We_{in}$  blocks the necking process of the outer droplet and delays the pinch-off time. Therefore, the interval of the external droplet inflation by penetration of the inner phase is increased, and the outer droplets become larger.

Increasing the middle phase capillary number causes the intermediate phase break-up location moving to the downstream due to the domination of the viscous forces over the interfacial forces, which results in the need for the larger interfacial tension force to overcome viscous force through larger middle phase droplets (Fig. 12b). However, the inner phase droplets will have smaller sizes as  $Ca_{mid}$  is increased (Fig. 12b). This is because the domination of the viscous forces of the middle phase results in higher viscous shear forces acting on the internal interface, which leads to the faster breakup of the inner droplets, and consequently, smaller droplet sizes.

The outer phase capillary increment reduces the size of both inner and outer droplets dramatically (Fig. 12c) due to the higher viscous drag force being acted on the external interface by the flow of the outer phase. This facilitates breakup of the middle phase jet and results in smaller outer droplets. On the other hand, the innermost interface has a lower dependency on  $Ca_{out}$ , since it is almost affected by the inner and outer

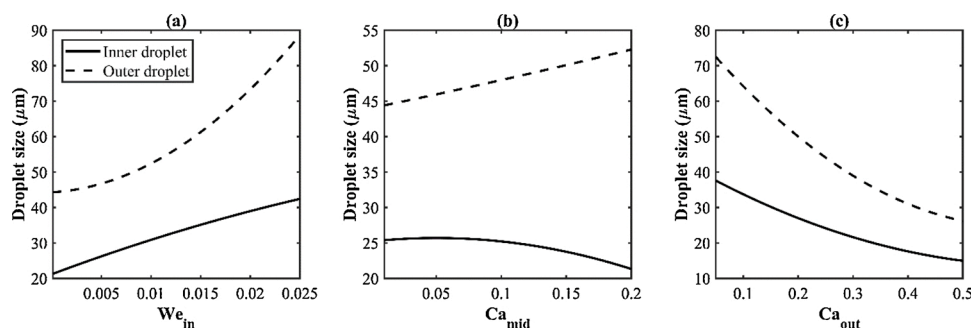


Fig. 12. The inner and outer droplet sizes as a function of (a)  $We_{in}$ , (b)  $Ca_{mid}$ , and (c)  $Ca_{out}$ .

phase parameters. Nevertheless, with increasing  $Ca_{out}$ , the inner droplets also have a smaller size due to the higher shear rate induced by the middle phase to the internal interface as a result of the intermediate phase jet suppression caused by the outer phase viscous effects.

Overall, the results of the non-dimensional analysis show a promising approach to detect the influence of various parameters on the double emulsion formation process. However, it should be considered that this approach cannot be utilized alone for the design of a compound droplet generation system without considering the influence of individual parameters, as illustrated by the sensitivity analysis.

#### 4. Conclusions

This paper simulated the generation of compound droplets in a dual-coaxial microfluidic device by altering phase velocities and physical properties using the VOF-CSF numerical model. The effects of each input parameter on the compound droplet characteristics, including inner and outer droplet size and frequency of formation, was examined using the design of experiments and response surface methodology. The local sensitivity analysis revealed that the external phase parameters have the most significant influence on compound droplet formation. It has also been shown that the characteristics of the inner phase droplet can be altered almost independently by tuning internal phase velocity and viscosity. However, changing the outer droplet diameter alone is a more arduous procedure. Also, three dimensionless groups of  $e_{in}$ ,  $Ca_{mid}$ , and  $Ca_{out}$  were implemented to investigate the effects of the effective forces on compound droplet size. Results ascertained that increasing  $We_{in}$  and  $Ca_{out}$  lead to the larger and smaller droplets, respectively, while increasing  $Ca_{mid}$  results in larger outer droplets and smaller inner droplets.

Overall, this study demonstrates the influence of phase physical properties and flow rates on compound droplet formation in a dual-coaxial microfluidic device, which can be applied to generate a broad range of liquid-liquid encapsulated structures (varies between 20 and 100  $\mu m$ ). Using the response surface methodology, one can easily extract required conditions (including physical properties of phases and phase flow rates) to obtain a specific size and aspect ratio of double emulsions. It is also possible to fix some input parameters (with the assumption that working fluids are previously selected) and obtain desired double emulsion characteristics by tuning other input parameters. Hence, it would be a beneficial tool for the applications requiring particular size, aspect ratio, and formation frequency of double emulsions, which considerably diminishes the challenging procedure of tuning physical properties and three phase flow rates in experimental work to achieve the desired results. More studies are required to extend the results to 3D geometries and also study the effects of geometrical ratios on double emulsion formation.

#### CRediT authorship contribution statement

Amirmohammad Sattari: Conceptualization, Methodology,

Software, Investigation, Writing - original draft, Formal analysis. Nishat Tasnim: Writing - review & editing, Validation, Data curation. Pedram Hanafizadeh: Conceptualization, Investigation, Project administration, Supervision, Writing - review & editing. Mina Hoofar: Writing - review & editing, Supervision, Project administration.

#### Declaration of Competing Interest

None.

#### References

- [1] S. Lee, J.-H. Ahn, H. Choi, J.M. Seo, D. Cho, K. Koo, Natural magnetic nanoparticle containing droplet for smart drug delivery and heat treatment, 2015 37th Annual International Conference of the IEEE Engineering in Medicine and Biology Society (EMBC) (2015) 3541–3544.
- [2] R. Riahi, A. Tamayol, S.A.M. Shaeigh, A.M. Ghaemmaghami, M.R. Dokmeci, A. Khademhosseini, Microfluidics for advanced drug delivery systems, *Curr. Opin. Chem. Eng.* 7 (2015) 101–112.
- [3] D. Chong, et al., Advances in fabricating double-emulsion droplets and their biomedical applications, *Microfluid. Nanofluidics* 19 (5) (2015) 1071–1090.
- [4] N.P. Aditya, S. Aditya, H. Yang, H.W. Kim, S.O. Park, S. Ko, Co-delivery of hydrophobic curcumin and hydrophilic catechin by a water-in-oil-in-water double emulsion, *Food Chem.* 173 (2015) 7–13.
- [5] G. Muschollik, Multiple emulsions for food use, *Curr. Opin. Colloid Interface Sci.* 12 (4–5) (2007) 213–220.
- [6] X. Li, X. Jiang, Microfluidics for producing poly (lactic-co-glycolic acid)-based pharmaceutical nanoparticles, *Adv. Drug Deliv. Rev.* 128 (2018) 101–114.
- [7] N. LiáJen, others, Microfluidic vascularized bone tissue model with hydroxyapatite-incorporated extracellular matrix, *Lab Chip* 15 (20) (2015) 3984–3988.
- [8] K. Yoshida, T. Sekine, F. Matsuzaki, T. Yanaki, M. Yamaguchi, Stability of vitamin A in oil-in-water-in-oil-type multiple emulsions, *J. Am. Oil Chem. Soc.* 76 (2) (1999) 1–6.
- [9] K. Miyazawa, I. Yajima, I. Kaneda, T. Yanaki, Preparation of a new soft capsule for cosmetics, *J. Cosmet. Sci.* 51 (4) (2000) 239–252.
- [10] S.M.S. Murshed, S.H. Tan, N.T. Nguyen, T.N. Wong, L. Yobas, Microdroplet formation of water and nanofluids in heat-induced microfluidic T-junction, *Microfluid. Nanofluidics* 6 (2) (2009) 253–259.
- [11] T. Fu, Y. Ma, D. Funschilling, C. Zhu, H.Z. Li, Squeezing-to-dripping transition for bubble formation in a microfluidic T-junction, *Chem. Eng. Sci.* 65 (12) (2010) 3739–3748.
- [12] I. Chakraborty, J. Ricouvier, P. Yazhgur, P. Tabeling, A.M. Leshansky, Droplet generation at Hele-shaw microfluidic T-junction, *Phys. Fluids* 31 (2) (2019) 22010.
- [13] S.L. Anna, N. Bontoux, H.A. Stone, Formation of dispersions using ‘flow focusing’ in microchannels, *Appl. Phys. Lett.* 82 (3) (2003) 364–366.
- [14] A.S. Utada, A. Fernandez-Nieves, H.A. Stone, D.A. Weitz, Dripping to jetting transitions in coflowing liquid streams, *Phys. Rev. Lett.* 99 (9) (2007) 94502.
- [15] N.M. Kovalchuk, E. Roumpea, E. Nowak, M. Chanaud, P. Angeli, M.J.H. Simmons, Effect of surfactant on emulsification in microchannels, *Chem. Eng. Sci.* 176 (2018) 139–152.
- [16] P. Thurgood, S. Baratchi, A. Arash, E. Pirogova, A.R. Jex, K. Khoshmanesh, Asynchronous generation of oil droplets using a microfluidic flow focusing system,” *Sci. Rep.* 9 (1) (2019) 1–11, <https://doi.org/10.1038/s41598-019-47078-8>.
- [17] M.L. Cordero, F. Gallaire, C.N. Baroud, Quantitative analysis of the dripping and jetting regimes in co-flowing capillary jets, *Phys. Fluids* 23 (9) (2011) 94111.
- [18] M.A. Herrada, A.M. Gañán-Calvo, A. Ojeda-Monge, B. Bluth, P. Riesco-Chueca, Liquid flow focused by a gas: jetting, dripping, and recirculation, *Phys. Rev. E Stat. Nonlinear Soft Matter Phys.* (2008), <https://doi.org/10.1103/PhysRevE.78.036323>.
- [19] A. Sattari, P. Hanafizadeh, M. Hoofar, Multiphase flow in microfluidics: from droplets and bubbles to the encapsulated structures, *Adv. Colloid Interface Sci.* 282 (2020), <https://doi.org/10.1016/j.cis.2020.102208>.



- [20] A.S. Utada, E. Lenceau, D.R. Link, P.D. Kaplan, H.A. Stone, D.A. Weitz, Monodisperse double emulsions generated from a microcapillary device, *Science* (80-) (2005), <https://doi.org/10.1126/science.1109164>.
- [21] K. Akamatsu, S. Kanasugi, S. Nakao, D.A. Weitz, Membrane-integrated glass capillary device for preparing small-sized water-in-oil-in-water emulsion droplets, *Langmuir* 31 (25) (2015) 7166–7172.
- [22] J.-O. Nam, J. Kim, S.H. Jin, Y.-M. Chung, C.-S. Lee, Microfluidic preparation of a highly active and stable catalyst by high performance of encapsulation of polyvinylpyrrolidone (PVP)-Pt nanoparticles in microcapsules, *J. Colloid Interface Sci.* 464 (2016) 246–253.
- [23] Y. Pang, Y. Du, J. Wang, Z. Liu, Generation of single/double Janus emulsion droplets in co-flowing microtube, *Int. J. Multiph. Flow* 113 (2019) 199–207, <https://doi.org/10.1016/j.ijmultiphaseflow.2019.01.011>.
- [24] S.A. Nabavi, G.T. Vladisavljević, V. Manović, Mechanisms and control of single-step microfluidic generation of multi-core double emulsion droplets, *Chem. Eng. J.* 322 (2017) 140–148, <https://doi.org/10.1016/j.cej.2017.04.008>.
- [25] R. Chen, P.-F. Dong, J.-H. Xu, Y.-D. Wang, G.-S. Luo, Controllable microfluidic production of gas-in-oil-in-water emulsions for hollow microspheres with thin polymer shells, *Lab Chip* 12 (20) (2012) 3858, <https://doi.org/10.1039/c2lc04387k>.
- [26] S.H. Kim, D.A. Weitz, One-step emulsification of multiple concentric shells with capillary microfluidic devices, *Angew. Chemie Int. Ed.* 50 (37) (2011) 8731–8734, <https://doi.org/10.1002/anie.201102946>.
- [27] A.R. Abate, J. Thiele, D.A. Weitz, One-step formation of multiple emulsions in microfluidics, *Lab Chip* 11 (2) (2011) 253–258, <https://doi.org/10.1039/c0lc00236d>.
- [28] C. Zhou, P. Yue, J.J. Feng, Formation of simple and compound drops in microfluidic devices, *Phys. Fluids* 18 (9) (2006) 1–14, <https://doi.org/10.1063/1.2353116>.
- [29] S.A. Nabavi, G.T. Vladisavljević, S. Gu, E.E. Ekanem, Double emulsion production in glass capillary microfluidic device: parametric investigation of droplet generation behaviour, *Chem. Eng. Sci.* 130 (2015) 183–196, <https://doi.org/10.1016/j.ces.2015.03.004>.
- [30] S.A. Nabavi, S. Gu, G.T. Vladisavljević, E.E. Ekanem, Dynamics of double emulsion break-up in three phase glass capillary microfluidic devices, *J. Colloid Interface Sci.* 450 (2015) 279–287, <https://doi.org/10.1016/j.jcis.2015.03.032>.
- [31] M. Azarmanesh, M. Farhadi, P. Azizian, Double emulsion formation through hierarchical flow-focusing microchannel, *Phys. Fluids* 28 (3) (2016), <https://doi.org/10.1063/1.4944058>.
- [32] T.V. Vu, S. Homma, G. Tryggvason, J.C. Wells, H. Takakura, Computations of breakup modes in laminar compound liquid jets in a coflowing fluid, *Int. J. Multiph. Flow* (2013), <https://doi.org/10.1016/j.ijmultiphaseflow.2012.10.004>.
- [33] A. Sattari, P. Hanafizadeh, Controlled preparation of compound droplets in a double rectangular co-flowing microfluidic device, *Colloids Surf. A Physicochem. Eng. Asp.* 602 (February) (2020) 125077, <https://doi.org/10.1016/j.colsurfa.2020.125077>.
- [34] P. Day, A. Manz, Y. Zhang, *Microdroplet Technology: Principles and Emerging Applications in Biology and Chemistry*, Springer Science & Business Media, 2012.
- [35] T.E. Tezduyar, Interface-tracking and interface-capturing techniques for finite element computation of moving boundaries and interfaces, *Comput. Methods Appl. Mech. Eng.* 195 (23–24) (2006) 2983–3000.
- [36] V.L. Srinivas, *Study of Interface Tracking and Capturing Methods*, INDIAN INSTITUTE OF TECHNOLOGY, MADRAS, 2016.
- [37] S. Bashir, J.M. Rees, W.B. Zimmerman, Simulations of microfluidic droplet formation using the two-phase level set method, *Chem. Eng. Sci.* (2011), <https://doi.org/10.1016/j.ces.2011.06.034>.
- [38] M. De Menech, Modeling of droplet breakup in a microfluidic T-shaped junction with a phase-field model, *Phys. Rev. E Stat. Nonlinear Soft Matter Phys.* (2006), <https://doi.org/10.1103/PhysRevE.73.031505>.
- [39] C.W. Hirt, B.D. Nichols, Volume of fluid (VOF) method for the dynamics of free boundaries, *J. Comput. Phys.* (1981), [https://doi.org/10.1016/0021-9991\(81\)90145-5](https://doi.org/10.1016/0021-9991(81)90145-5).
- [40] J.U. Brackbill, D.B. Kothe, C. Zemach, A continuum method for modeling surface tension, *J. Comput. Phys.* (1992), [https://doi.org/10.1016/0021-9991\(92\)90240-Y](https://doi.org/10.1016/0021-9991(92)90240-Y).
- [41] S.A. Nabavi, G.T. Vladisavljević, M.V. Bandulasena, O. Arjmandi-Tash, V. Manović, Prediction and control of drop formation modes in microfluidic generation of double emulsions by single-step emulsification, *J. Colloid Interface Sci.* 505 (2017) 315–324, <https://doi.org/10.1016/j.jcis.2017.05.115>.
- [42] S. Mukherjee, A. Zarghami, C. Haringa, K. van As, S. Kenjeres, H.E.A. Van den Akker, Simulating liquid droplets: a quantitative assessment of lattice Boltzmann and Volume of Fluid methods, *Int. J. Heat Fluid Flow* 70 (December) (2018) 59–78, <https://doi.org/10.1016/j.ijheatfluidflow.2017.12.001>.
- [43] M. Eswaran, U.K. Saha, D. Maity, Effect of baffles on a partially filled cubic tank: numerical simulation and experimental validation, *Comput. Struct.* 87 (3–4) (2009) 198–205.
- [44] S. Nicolici, R.M. Bilegan, Fluid structure interaction modeling of liquid sloshing phenomena in flexible tanks, *Nucl. Eng. Des.* 258 (2013) 51–56.
- [45] D. Wang, C. Wu, W. Huang, Y. Zhang, Vibration investigation on fluid-structure interaction of AP1000 shield building subjected to multi earthquake excitations, *Ann. Nucl. Energy* 126 (2019) 312–329.
- [46] J.-P. Aubry, *Beginning with Code\_Aster, A Pract. Introd. to Finite Elem. Method Using Code\_Aster*, Gmsh Salome. Fram., 2013.
- [47] D. Thakore, *Finite Element Analysis with Open Source Software*, Moonish Enterprises, 2013.
- [48] T. Shao, X. Feng, Y. Jin, Y. Cheng, Controlled production of double emulsions in dual-coaxial capillaries device for millimeter-scale hollow polymer spheres, *Chem. Eng. Sci.* 104 (2013) 55–63, <https://doi.org/10.1016/j.ces.2013.09.001>.
- [49] M.J. Anderson, P.J. Whitcomb, Design of experiments, *Kirk-Othmer Encycl. Chem. Technol.* (2000) 1–22.
- [50] P.A.J. Rosa, A.M. Azevedo, M.R. Aires-Barros, Application of central composite design to the optimisation of aqueous two-phase extraction of human antibodies, *J. Chromatogr. A* (2007), <https://doi.org/10.1016/j.chroma.2006.11.075>.
- [51] M. Ahmadi, F. Vahabzadeh, B. Bonakdarpour, E. Mofarrah, M. Mehranian, Application of the central composite design and response surface methodology to the advanced treatment of olive oil processing wastewater using Fenton's peroxidation, *J. Hazard. Mater.* (2005), <https://doi.org/10.1016/j.jhazmat.2005.03.042>.
- [52] C.G. Bucher, U. Bourgund, A fast and efficient response surface approach for structural reliability problems, *Struct. Saf.* (1990), [https://doi.org/10.1016/0167-4730\(90\)90012-E](https://doi.org/10.1016/0167-4730(90)90012-E).
- [53] R.H. Myers, D.C. Montgomery, C.M. Anderson-Cook, *Response Surface Methodology: Process and Product Optimization Using Designed Experiments*, John Wiley & Sons, 2016.
- [54] H.R.F. Masoumi, M. Basri, W.S. Samiun, Z. Izadiyan, C.J. Lim, Enhancement of encapsulation efficiency of nanoemulsion-containing aripiprazole for the treatment of schizophrenia using mixture experimental design, *Int. J. Nanomed.* (2015), <https://doi.org/10.2147/IJN.S89364>.
- [55] B.D. Hamlington, B. Steinhaus, J.J. Feng, D. Link, M.J. Shelley, A.Q. Shen, Liquid crystal droplet production in a microfluidic device, *Liq. Cryst.* 34 (7) (2007) 861–870, <https://doi.org/10.1080/02678290601171485>.
- [56] M.L. Cordero, F. Gallaire, C.N. Baroud, Quantitative analysis of the dripping and jetting regimes in co-flowing capillary jets, *Phys. Fluids* 23 (9) (2011), <https://doi.org/10.1063/1.3634044>.
- [57] A.S. Utada, A. Fernandez-Nieves, H.A. Stone, D.A. Weitz, Dripping to jetting transitions in coflowing liquid streams, *Phys. Rev. Lett.* 99 (9) (2007) 1–4, <https://doi.org/10.1103/PhysRevLett.99.094502>.
- [58] R. Suryo, P. Doshi, O.A. Basaran, Nonlinear dynamics and breakup of compound jets, *Phys. Fluids* (2006), <https://doi.org/10.1063/1.2245377>.